ACS APPLIED MATERIALS & INTERFACES

Research Article

www.acsami.org

# Layer-by-Layer Deposition of Organic–Inorganic Hybrid Multilayer on Microporous Polyethylene Separator to Enhance the Electrochemical Performance of Lithium-Ion Battery

Wuxia Xu,[†] Zhuyi Wang,*[,†] Liyi Shi,[†] Ying Ma,[‡] Shuai Yuan,*[,†] Lining Sun,[†] Yin Zhao,[†] Meihong Zhang,[†] and Jiefang Zhu[§]

[†]Research Centre of Nanoscience and Nanotechnology, Shanghai University, Shanghai 200444, China

[‡]Donghua University, Shanghai 201620, China

[§]Ångström Advanced Battery Centre, Uppsala University, 75121 Uppsala, Sweden

Supporting Information

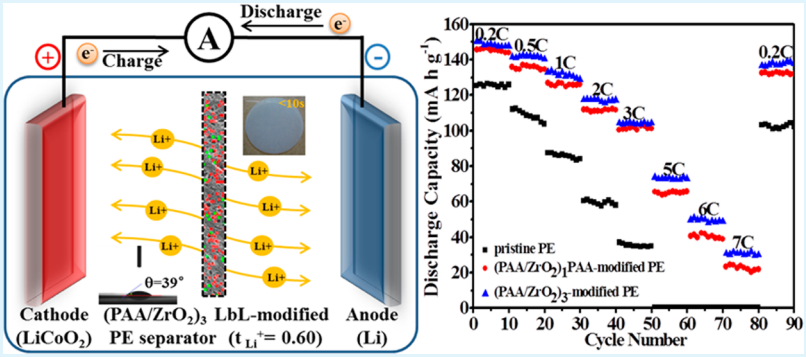


**ABSTRACT:** A simple layer-by-layer (LbL) self-assembly process of poly(acrylic acid) (PAA) and $ZrO_2$ was applied to construct functional ultrathin multilayers on polyethylene (PE) separators without sacrificing the excellent porous structure of separators. Such PAA/$ZrO_2$ LbL-modified PE separators possess good electrolyte wettability, excellent electrolyte uptake, high ionic conductivity and large $Li^+$ transference number. More importantly, the top layer of LbL self-assembly would affect the dissociation of electrolyte and the formation of solid electrolyte interphase (SEI) layer in half-cells. Compared with the pristine and $(PAA/ZrO_2)_1$PAA-modified PE separators, $(PAA/ZrO_2)_3$-modified PE separator shows a larger $Li^+$ transference number (0.6) and a faster tendency to form a stable SEI layer, endowing half-cells with excellent capacity retention at high C-rates and superior cycling performance. These fascinating characteristics will provide the LbL self-assembly with a promising method to improve the surface property of PE separators for high performance lithium-ion batteries.

**KEYWORDS:** *layer-by-layer self-assembly, surface modification, separator, Li-ion battery, C-rate capability*

## 1. INTRODUCTION

In recent years, there has been a strong demand for lithium-ion batteries (LIBs) with excellent energy density and cycle life due to the strong growth in portable electronics, hybrid electric vehicles, and utility grids.[1−3] This requires the properties of all cell components (i.e., electrode materials, separators, and electrolytes) to be further improved. The essential function of a separator is to keep the positive and negative electrodes apart to prevent electrical short circuits in batteries and at the same time allow rapid $Li^+$ ion transport. So, it plays a vital role in LIBs due to its close connection with the electrochemical performance and safety of cells, and becomes a big concern for large-scale applications of LIBs.[4,5] Currently, the most widely used separators in LIBs are made of polyolefin materials, such as polyethylene (PE) and polypropylene (PP) due to their acceptable cost, proper pore structure, good mechanical strength, and favorable thermal shutdown property. However, the major disadvantages of these polyolefin separators lie in their intrinsically hydrophobic surface character, which results in poor wettability and retention to polar liquid electrolyte. As a result, the migration of $Li^+$ ions through polyolefin separators is impaired, which adversely affects the electrochemical energy efficiency of the batteries. Moreover, the thermal stability of polyolefin separators also needs to be further enhanced to provide a greater margin of safety for LIBs during overcharge or abnormal heating conditions.

To overcome these drawbacks of commercial polyolefin separators, various surface modification approaches have been tried, such as plasma treatment, graft polymerization, dip-coating and impregnation of a gel polymer electrolyte.[6−10]

Received: June 19, 2015
Accepted: September 3, 2015
Published: September 3, 2015





DOI: 10.1021/acsami.5b05457
ACS Appl. Mater. Interfaces 2015, 7, 20678−20686

**Scheme 1. (a) Cross-Sectional Diagram of Pristine and PAA/$ZrO_2$ LbL-Modified PE Separators and (b) Layer-by-Layer Self-Assembly Process for the Construction of PAA/$ZrO_2$ Multilayers on PE Separator**

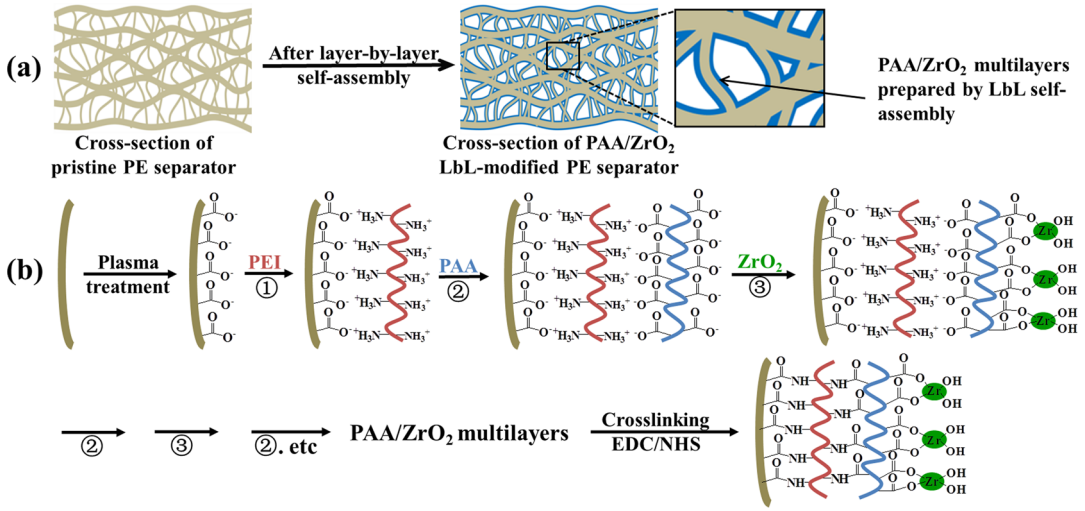


Among them, the dip-coating of some organic polymers or inorganic oxides with excellent thermal stability and good hydrophilicity on the surface of separators has been extensively studied to improve the thermal stability and electrolyte uptake of separators.[9,11−17] However, dip-coating method also generates inevitable negative effects, such as the significantly increased thickness,[14] seriously blocked porous structure[12] and unmodified inner pores of separators. The thicker separators take up more space and decrease the volume of active materials that can be placed inside the battery, and the blocked pores hinder the transport of $Li^+$ ions, which is unfavorable for the cell electrochemical performance.[4,5] So it is anticipated to find new modification methods that can optimize the wettability and electrochemical performance of polyethylene separator without sacrificing its excellent microporous structure.

Layer-by-layer (LbL) self-assembly via alternate adsorption of various functional building blocks driven by specific intermolecular interactions has been developed to fabricate supramolecular hybrid multilayers with tunable architecture and properties.[18] This method is simple and versatile and allows the integration of various functional structures for a specific application. Especially, it offers the ability to exert molecular-level control over the composition, surface characteristics and thickness of the assembled multilayer. Inspired by the inherent advantages of LbL self-assembly, we attempted to modify polyethylene (PE) separators with organic−inorganic hybrid supramolecular multilayers deposited by LbL self-assembly. Furthermore, the effects of supramolecular multilayers on the crucial physical and electrochemical properties of PE separator and the performance of lithium-ion half-cells ($LiCoO_2$ /Li metal) were investigated and discussed in detail.

## 2. EXPERIMENTAL SECTION

**2.1. Materials.** A commercial polyethylene (PE) separator (thickness, 14 $\mu$m; porosity, 52%) was purchased from SK Energy Company (Seoul, Korea). Poly(acrylic acid) (PAA, $M_w$ = 1800 g $mol^{-1}$), branched-poly(ethylenimine) (PEI, $M_w$ = 25000 g $mol^{-1}$), 2-morpholinoethanesulfonic acid (MES), 1-ethyl-3-(3-(dimethylamino)-propyl) carbodimide (EDC) and *N*-hydroxysulfosuccinimide sodium salt (NHS) were purchased from Sigma-Aldrich. All these chemicals were used as received without further purification. Colloidal $ZrO_2$ nanoparticles were prepared according to our previous work.[19] Lithium metal foil was obtained from China Energy Lithium Company (Tianjin, China). The liquid electrolyte containing $LiPF_6$ (1 mol $L^{-1}$) in a mixture of ethylene carbonate (EC)/ethyl methyl carbonate (EMC)/dimethyl carbonate (DMC) (1:1:1, by volume) was purchased from Guotai Huarong Company (Zhangjiagang, China).

**2.2. Preparation of PAA/$ZrO_2$ LbL-Modified PE Separators.** The preparation process of PAA/$ZrO_2$ LbL-modified PE separators is illustrated in Scheme 1. First, PE separators were treated with $CO_2$-plasma (power, 80 W; time, 60 s) to generate a carboxylic surface capable of undergoing charge or hydrogen bond interactions.[20,21] Then the resulting PE separators were immersed in a PEI solution (1 mg $mL^{-1}$) for 20 min followed by rinse to obtain a PEI primer layer. Subsequently, the PEI-primed PE separators were alternatively dipped into a PAA solution (0.03 mg $mL^{-1}$) and a $ZrO_2$ colloid (1 mg $mL^{-1}$) with desired cycle number to allow the alternative adsorption of PAA and $ZrO_2$. The dipping time in the PAA solution or $ZrO_2$ colloid was 10 min, and each dipping step was followed by the rinse process. The pH values of PAA solution and $ZrO_2$ colloid were adjusted to 3.5 with HCl (1 mol $L^{-1}$) aqueous solution. All deposition and rinse solutions used for the buildup of PAA/$ZrO_2$ multilayers were a mixture of water and methanol (3:7 v/v). Here, the PAA/$ZrO_2$ multilayers with a desired cycle number n is noted as $(PAA/ZrO_2)_n$ or $(PAA/ZrO_2)_nPAA$, which means the top layer of modification is $ZrO_2$ or PAA, respectively.

The sequential deposition of PEI and PAA is driven by the electrostatic force, and the alternative deposition of PAA/$ZrO_2$ is driven by coordination chemistry interactions between −COOH and $ZrO_2$. A follow-up step after self-assembly is to immerse the PAA/$ZrO_2$ LbL-modified PE separators into a solution of EDC (0.1 mol $L^{-1}$) and NHS (0.1 mol $L^{-1}$) in MES buffer [0.05 mol $L^{-1}$, pH 5.5, water/methanol (3:7 v/v) as solvent] for 12 h to undergo the cross-linking of PEI/separator and PAA/PEI interlayers through the imidization between carboxyl and amino groups.[20]

**2.3. Characterization of PAA/$ZrO_2$ LbL-Modified PE Separators.** A quartz crystal microbalance (QCM) device (Agilent, 53131A) with a frequency counter was used to determine the deposited mass after each adsorption step. The Ag-coated QCM resonators were cleaned by sequential dipping into acetone (30 min), alcohol (30 min), and water (30 min), and then dried with nitrogen. Scanning electron microscopy (SEM) combined with energy dispersive X-ray spectroscopy (EDS) (JEOL, 6700F) was used to examine the surface and cross-sectional porous structure of separators as well as the elemental distribution. The air permeability of separators was examined with a Gurley densometer (UEC, 1012A) by measuring the time for 100 cc of air to pass through under a given pressure. Water contact angle measurement was performed using a drop shape analyzer (KRUSS, DSA100). The electrolyte uptake was obtained by


DOI: 10.1021/acsami.5b05457
ACS Appl. Mater. Interfaces 2015, 7, 20678−20686

measuring the weight of separators before and after soaking in liquid electrolyte for 1 h and then calculated using the following equation:

$$\text{uptake}\ (\%) = \frac{(W_t - W_0)}{W_0} \times 100 \quad (1)$$

where $W_0$ and $W_t$ represent the weight of separators before and after soaking in the liquid electrolyte, respectively. The thermal shrinkage of separators was determined by measuring the dimensional change of them after the thermal treatment at different temperatures for 0.5 h.

**2.4. Electrochemical Analysis.** The ionic conductivity was measured by AC impedance spectra using an electrochemical working station (Chenhua, CHI660E) in the frequency range of 10 mHz to 1 MHz at 25 °C. The liquid electrolyte-saturated separators were sandwiched between two stainless steel (SS) electrodes (diameter, 1.7 cm) and assembled into a blocking-type cell. The ionic conductivity was calculated according to the equation

$$\sigma = R_b^{-1} S^{-1} d \quad (2)$$

where $\sigma$ represents ionic conductivity, $R_b$ is the bulk resistance, $S$ is the geometric area of stainless steel electrodes, and $d$ is the thickness of separators.

The $Li^+$ transference number was determined by the combination of chronoamperometry and AC impedance analysis of Li/separator/Li cells. The chronoamperometry profile was monitored at a constant potential (10 mV) for 1000 s and the AC impedance spectra were measured before and after polarization. The $Li^+$ transference number was calculated by the following equation:

$$t_{Li^+} = \frac{I_s(\Delta V - I_0 R_0)}{I_0(\Delta V - I_s R_s)} \quad (3)$$

where $I_0$ and $I_s$ are the initial and steady-state current determined by the chronoamperometry; $\Delta V$ is the potential difference (10 mV); $R_0$ and $R_s$ are the interfacial resistance before and after polarization measured by AC impedance spectra.

The electrochemical stability window of separators was evaluated by the linear sweep voltammetry (LSV) test performed on SS/separator/Li cells at a scan rate of 5 mV/s between 0 and 6 V (vs $Li^+$/Li). The stainless steel was used as the working electrode, and Li metal foil was used as the counter and reference electrodes.

The interfacial resistance ($R_{int}$) between separators and Li metal electrodes was measured by monitoring the AC impedance response of Li/separator/Li cells over storage up to 8 days. The measurements were carried out over the frequency range of 10 mHz to 1 MHz at 25 °C.

Charge−discharge cycle tests of $LiCoO_2$/separator/Li half-cells were performed at indicated current densities in the voltage range of 3.0 to 4.2 V using a LANHE Battery Testing System (Wuhan Land, CT2001A). The $LiCoO_2$ electrodes were prepared by mixing the $LiCoO_2$ powder (80 wt %), carbon black (10 wt %), and PVDF (10 wt %) in *N*-methylpyrrolidone (NMP) solvent. The mixed slurry was coated on aluminum foil and dried at 120 °C for 24 h. The electrode disks (0.7854 $cm^2$) were then punched out of the coated aluminum foils and weighted. $LiCoO_2$/separator/Li half-cells were fabricated with 2016-coin type cells in the argon-filled glovebox (MBRAUM, W13006-2). For the cycle capability measurements, all the half-cells were cycled at 0.2 C (0.14 mA $cm^{-2}$). For the rate capability measurements, all the half-cells were cycled at current rates of 0.2 to 7 C. The electrochemical impedance of the half-cells was also measured on the electrochemical working station in the frequency range of 10 mHz to 1 MHz at 25 °C.

## 3. RESULTS AND DISCUSSION

**3.1. Layer-by-Layer Self-Assembly of PAA/$ZrO_2$ Multilayers on Microporous Polyethylene Separators.** The fabrication of PAA/$ZrO_2$ multilayers was monitored by the quartz crystal microbalance (QCM). As shown in Figure 1, QCM frequency change ($-\Delta F$) presents a regular linear growth with the alternate deposition of PAA and $ZrO_2$ on QCM resonator. The frequency change is 225.5 ± 52.3 Hz for PAA adsorption and 289.4 ± 43.4 Hz for $ZrO_2$, corresponding to 203.0 ± 47.1 and 260.5 ± 39.1 ng (1 Hz decrease corresponds to a mass increase of 0.9 ng), respectively. These results clearly demonstrate that PAA and $ZrO_2$ can be successfully assembled through the LbL self-assembly method.

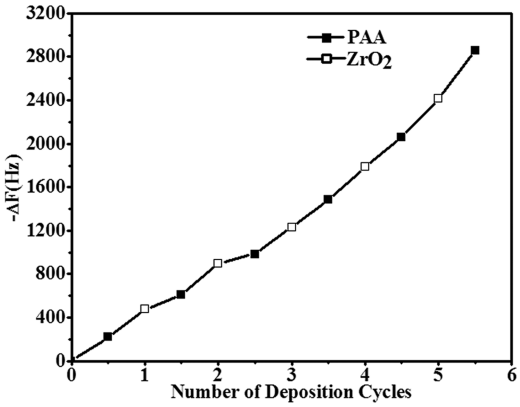


**Figure 1.** QCM frequency change ($-\Delta F$) for the alternate deposition of PAA and $ZrO_2$.

The surface and cross-sectional SEM images of pristine and modified PE separators are shown in Figure 2. No obvious change in the porous structure and the thickness of separators before and after LbL modification was observed, which suggests that this method can minimize the thickness increase of PE separator and preserve the porous structure to the maximum. This well-preserved porous character was also analyzed quantitatively by measuring the Gurley values of pristine and modified PE separators. As shown in Table 1, the Gurley values of modified PE separators increase slightly with the increasing deposition cycles due to the molecular-level control over the layer thickness of the LbL self-assembly. In order to investigate the distribution of PAA/$ZrO_2$ multilayers on PE separator, the energy dispersive X-ray spectroscopy (EDS) was analyzed for $(PAA/ZrO_2)_3$-modified PE separator (Figure 3). The homogeneous distribution of Zr and O throughout the surface and cross-section of $(PAA/ZrO_2)_3$-modified PE separators confirms that PAA/$ZrO_2$ multilayers were successfully assembled throughout both the outer and inner surfaces of PE separators.

**3.2. Physical and Electrochemical Properties of Modified Polyethylene Separators.** Various characterizations are used to analyze the effects of PAA/$ZrO_2$ LbL self-assembly on the surface structure and properties of modified PE separators. According to the results in Table 1 and Figure S1, the significantly decreased water contact angle of PE separator after PAA/$ZrO_2$ LbL self-assembly indicates the enhanced surface polarity and hydrophilicity, which will be helpful for PE separator to improve the electrolyte wetting capability. As shown in the liquid electrolyte absorption test (Figure S2), the pristine PE separator is hardly wetted by the liquid electrolyte because of its hydrophobic surface character and low surface energy. In contrast, the modified PE separators could be fully wetted in 10 s. The enhanced electrolyte wetting capability leads to the significantly increased electrolyte uptake from 120% (pristine PE separator) to 325% ($(PAA/ZrO_2)_3$-modified PE separator) (Table 1). In addition to the increased electrolyte uptake, it has also been found that all PAA/$ZrO_2$ LbL-modified PE separators have a reduced thermal shrinkage than the pristine PE separator over a wide range of


DOI: 10.1021/acsami.5b05457
ACS Appl. Mater. Interfaces 2015, 7, 20678−20686

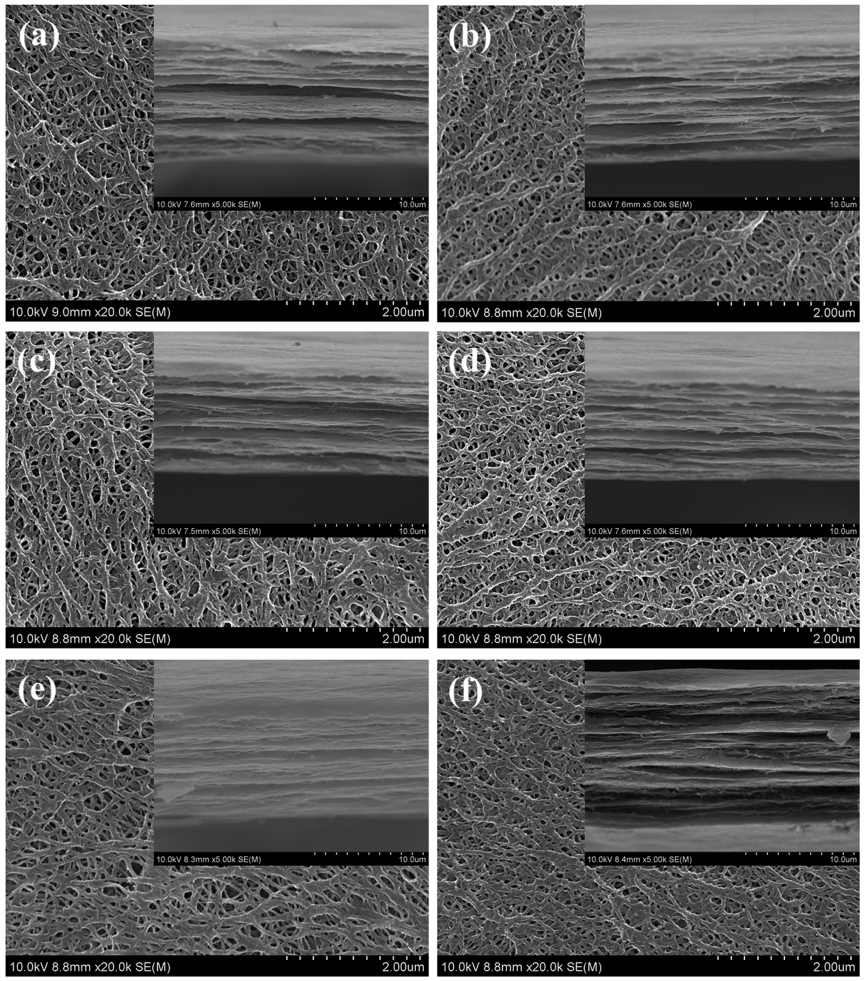


**Figure 2.** Surface SEM micrographs of different separators: (a) pristine PE, (b) $(PAA/ZrO_2)_1$-modified PE, (c) $(PAA/ZrO_2)_1PAA$-modified PE, (d) $(PAA/ZrO_2)_3$-modified PE, (e) $(PAA/ZrO_2)_3PAA$-modified PE, (f) $(PAA/ZrO_2)_5$-modified PE. (Insets) Cross-sectional micrographs of separators.

**Table 1. Physical and Electrochemical Properties of Pristine and Modified PE Separators**

| sample | Gurley value (s) | contact angle (deg) | electrolyte uptake (%) | ionic conductivity (mS $cm^{-1}$) | $Li^+$ transference number |
|---|---|---|---|---|---|
| pristine PE | 223 | 114 | 120 | 0.36 | 0.37 |
| $(PAA/ZrO_2)_1$-modified PE | 235 | 47 | 243 | 0.50 | 0.53 |
| $(PAA/ZrO_2)_1PAA$-modified PE | 237 | 49 | 230 | 0.41 | 0.43 |
| $(PAA/ZrO_2)_3$-modified PE | 242 | 39 | 325 | 0.51 | 0.60 |
| $(PAA/ZrO_2)_3PAA$-modified PE | 244 | 41 | 310 | 0.40 | 0.41 |
| $(PAA/ZrO_2)_5$-modified PE | 254 | 38 | 320 | 0.44 | 0.47 |

temparatures (Figure S3). This improvement in the thermal shrinkage is attributed to the presence of heat resistant $ZrO_2$ layers on the PE matrix, which plays a positive role in holding the overall skeleton of PE separator to resist against thermal shrinkage.

Figure 4 shows the Nyquist plots of SS/separator/SS cells based on pristine and modified PE separators at 25 °C. The high-frequency intercept on the real axis reflects the bulk resistance ($R_b$), which can be used to calculate the ionic conductivity in Table 1. According to the results, all $PAA/ZrO_2$ LbL-modified PE separators show higher ionic conductivity than the pristine PE separator, and the highest ionic conductivity was observed for $(PAA/ZrO_2)_3$-modified PE separator, which may benefit from the synergistic contributions of the significantly increased electrolyte uptake and the well-preserved porous structure. Interestingly, $(PAA/ZrO_2)_n$-modified PE separators show higher ionic conductivity than $(PAA/ZrO_2)_nPAA$-modified PE separators, indicating the effects of top layer on the ionic conductivity.

The $Li^+$ transference number (Table 1) obtained by the combination of chronoamperometry and AC impedance analysis (Figure 5) also follow the same trend as the ionic conductivity. All $PAA/ZrO_2$ LbL-modified PE separators show higher $Li^+$ transference number than pristine PE separator, and $ZrO_2$ as the top layer is more favorable for increasing the $Li^+$ transference number. These results reveal the trapping effects of electrolyte anions by $ZrO_2$, which allows more free $Li^+$ ions to be available for the conduction. Actually, it has been reported that inorganic fillers can act as the active Lewis acidic sites to capture anions in electrolyte.[22] It should be the Lewis acid–base interaction between $ZrO_2$ and $PF_6^-$ ions that promote the liquid electrolyte dissociation for higher ionic conductivity and


DOI: 10.1021/acsami.5b05457
ACS Appl. Mater. Interfaces 2015, 7, 20678–20686

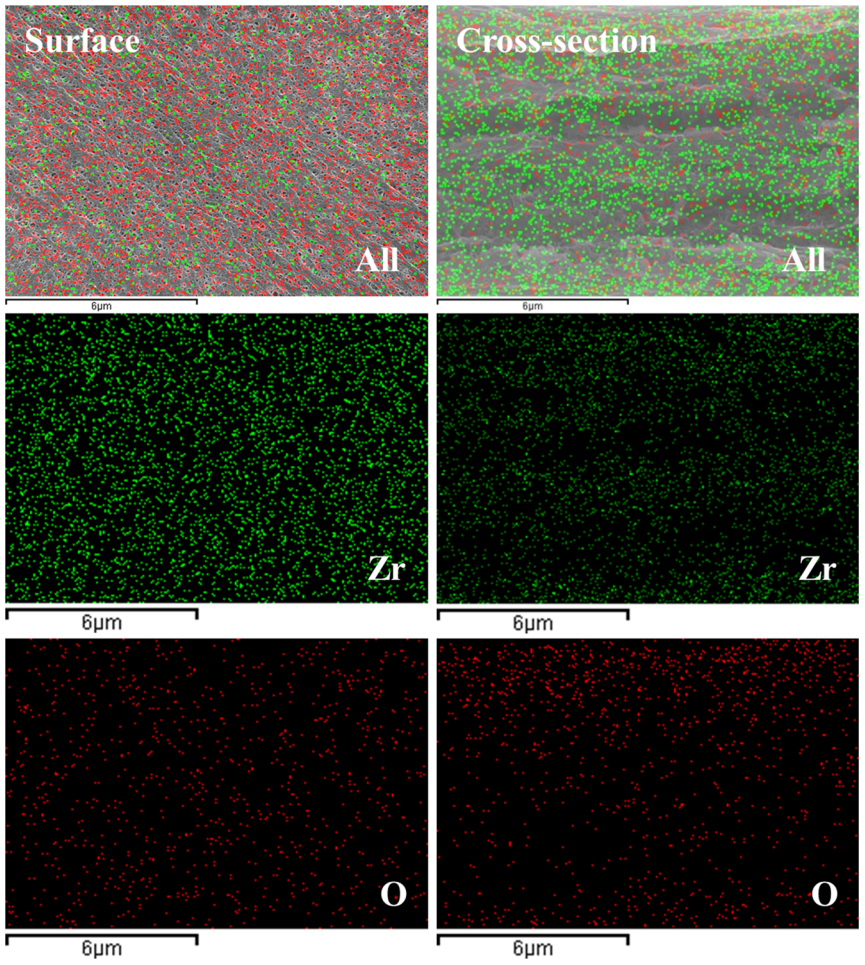


**Figure 3.** EDS elemental map of the surface and cross-section for $(PAA/ZrO_2)_3$-modified PE separator.

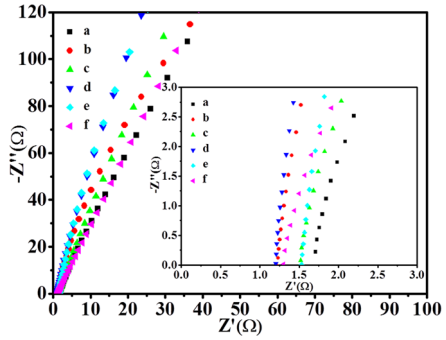


**Figure 4.** Nyquist plots of SS/separator/SS cells based on different separators at 25 °C: (a) pristine PE; (b) $(PAA/ZrO_2)_1$-modified PE; (c) $(PAA/ZrO_2)_1$PAA-modified PE; (d) $(PAA/ZrO_2)_3$-modified PE; (e) $(PAA/ZrO_2)_3$PAA-modified PE; and (f) $(PAA/ZrO_2)_5$-modified PE.

$Li^+$ transference number of modified PE separators using $ZrO_2$ as the top layer.[23]

The oxidative decomposition of electrolyte on cathode is one major cause for the safety problem of lithium-ion batteries,[24] which can be understood by the electrochemical stability window on stainless steel (SS) electrode. Figure S4 presents the linear sweep voltammetry (LSV) profiles of SS/separator/Li cells based on the pristine PE and modified PE separators. It is noticed that the electrochemical stability for the pristine PE is up to 4.4 V, while all modified PE separators have wider electrochemical stability windows, which may originate from the decreased free solvent molecules in liquid electrolyte to be decomposed on cathode led by the excellent electrolyte uptake,[25] and the stabilization of electrolyte anions by the trapping effect of $ZrO_2$ layer. Using the results mentioned above, we can fine tune the surface characteristic and electrochemical properties of PE separator by choosing the different building blocks as the top layer of LbL self-assembly. $(PAA/ZrO_2)_1$PAA-modified PE separator and $(PAA/ZrO_2)_3$-modified PE separator were chosen as representative samples to discuss the effects of different surface top layers of PE separator on electrochemical performance of lithium-ion battery.

**3.3. Battery Performance.** The discharge voltage profiles of half-cells assembled with the pristine PE separator, $(PAA/ZrO_2)_1$PAA-modified PE separator and $(PAA/ZrO_2)_3$-modified PE separator are shown in Figure 6a–c, and Figure 6d summarizes the discharge C-rate capacities of these three separators. It is worth noting that the half-cells assembled with both of $(PAA/ZrO_2)_1$PAA-modified PE separator and $(PAA/ZrO_2)_3$-modified PE separator exhibit much higher discharge capacities than pristine PE separator over various discharge current densities from 0.2 to 7 C. The half-cell assembled with pristine PE separator starts to lose all the capacity when the current density reaches 5 C. In contrast, the half-cells assembled with $(PAA/ZrO_2)_1$PAA-modified PE separator and $(PAA/ZrO_2)_3$-modified PE separator still hold 44.8 and 49.3% of the discharge capacity at 0.2 C, respectively. It is also found


DOI: 10.1021/acsami.5b05457
ACS Appl. Mater. Interfaces 2015, 7, 20678–20686

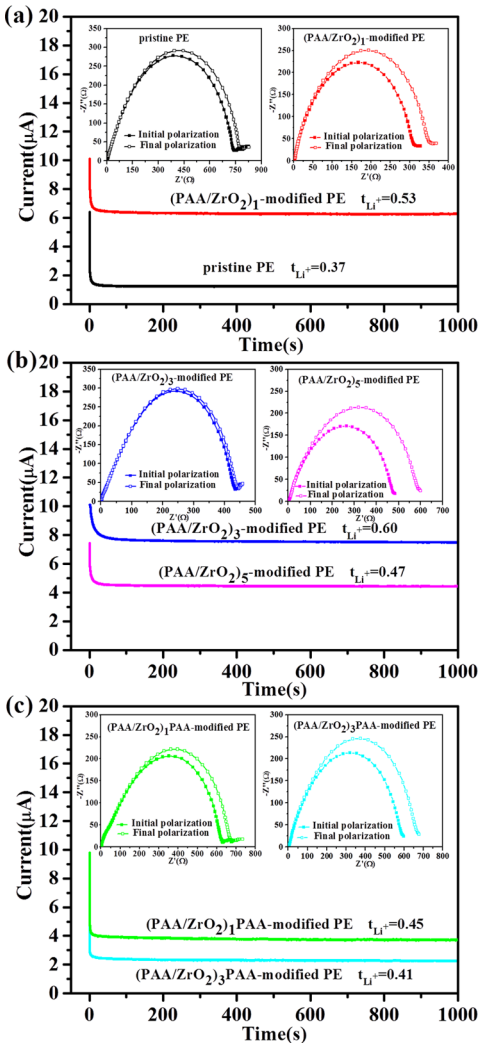


**Figure 5.** Chronoamperometry profiles and AC impedance analyses of Li/separator/Li cells based on the pristine and modified PE separators.

that the half-cells assembled with $(PAA/ZrO_2)_3$-modified PE separator show higher capacity especially under high discharge current densities (5−7 C) than $(PAA/ZrO_2)_1$PAA-modified PE separator, demonstrating the effects of surface top layer of PE separator on the capacity of cells. Typical cycle performance of half-cells assembled with these three separators is shown in Figure S5. Discharge capacity retentions of half-cells using $(PAA/ZrO_2)_1$PAA-modified and $(PAA/ZrO_2)_3$-modified PE separators are kept at 81.4 and 85.1% after 100 cycles, respectively, showing higher capacity retentions than pristine PE separator (76.0%). The homogeneous distribution of Zr and O throughout the surface (both of $LiCoO_2$ electrode side and Li electrode side) of $(PAA/ZrO_2)_3$-modified PE separators disassembled from cells after 50 cycles gives the evidence of the stability of PAA/$ZrO_2$ mutilayers on PE separators upon the frequent charge−discharge process (Figure S6).

AC impedance spectroscopy analysis was carried out in order to understand the effects of PAA/$ZrO_2$ multilayers on PE separator surface on the battery performance. The Nyquist plots of the half-cells assembled with the pristine PE separator, $(PAA/ZrO_2)_1$PAA-modified PE separator and $(PAA/ZrO_2)_3$-modified PE separator after the first and 50th cycle are presented in Figure 7, respectively. Nyquist plots of all the half-cells are clearly composed of two semicircles and an inclined line. The semicircle in the high frequency range (left) corresponds to the resistance due to $Li^+$ migration through SEI layer ($R_{SEI}$), the semicircle in the medium to low frequency range (right) corresponds to the charge transfer resistance at the electrode−electrolyte interfaces ($R_{ct}$), and the inclined line at low frequency represents the Warburg impedance of lithium ion diffusion into the active mass ($W_0$). The intercept at real axis corresponds to the combination resistance $R_e$ associated with the ionic conductivity of electrolyte, the intrinsic resistance of the cathode, separator, and anode, and the contact resistance at the electrode/current collector interface.[26−29] The sum of $R_e$, $R_{SEI}$, and $R_{ct}$ reflects the overall internal resistance of cells, and the decay of the discharge capacity with increasing the C-rates or cycle number is related to increased cell internal resistance. According to the resistance values shown in Table 2, $R_e$ is 1−2 magnitudes lower than $R_{SEI}$ and $R_{ct}$, and is negligible in the total resistance. So, $R_{SEI}$ and $R_{ct}$ are considered to be the leading factors influencing the discharge capacity of the battery. The half-cells assembled with PAA/$ZrO_2$ LbL-modified PE separators show much lower $R_{SEI}$ and $R_{ct}$ as cell cycles. Specially, the $R_{SEI}$ of the half-cells assembled with $(PAA/ZrO_2)_3$-modified PE separator increases only 2 Ω after 50 cycles, which means a suppressed and more stable formation of SEI-layer, facilitating lithium ion transport through SEI layer. More evidence of good SEI stability can be found by the compatibility analysis between separators and lithium electrode.

Figure 8 shows the AC impedance variation of symmetrical Li/separator/Li cells over different storage time. The distance between semicircle intercepts on the real axis corresponds to the value of interfacial resistance ($R_{int}$),[30] which is associated with the SEI layer and the charge transfer reaction $Li^+ + e^- = Li$ on the lithium electrode. According to the results, the initial $R_{int}$ of $(PAA/ZrO_2)_3$-modified PE separator is much smaller (483.6 Ω) than $(PAA/ZrO_2)_1$PAA-modified PE separator (692.7Ω) and pristine PE separator (797.6 Ω), and it quickly reaches stable after 5 days. However, the $R_{int}$ of pristine PE separator shows a continuous and rapid increase with storage time. The increase of $R_{int}$ with storage time is inevitable and it indicates the formation and growth of the SEI layer on the lithium electrode surface as a result of the reaction with electrolyte components.[22] The smaller and more quickly stabilized $R_{int}$ reflects better interfacial stability between the liquid electrolyte-soaked separator and the lithium electrode with continued storage. Compared to the pristine PE separator, $(PAA/ZrO_2)_1$PAA-modified and $(PAA/ZrO_2)_3$-modified PE separators show much higher electrolyte uptake, which reduces the amount of liquid electrolyte in contact with the lithium electrode for reaction. As for the difference between $(PAA/ZrO_2)_1$PAA-modified PE separator and $(PAA/ZrO_2)_3$-modified PE separator, $ZrO_2$ as the top layer provides Lewis acid sites to trap electrolyte anions, and the high surface area of $ZrO_2$ nanoparticles can also effectively hold the electrolyte solution by capillary force.[31] Once the interactions between the electrolyte and the lithium electrode are inhibited, the growth rate of the SEI layer will be slowed down. Moreover, $ZrO_2$ can also scavenge HF in the electrolyte[32] to prevent the attack of HF toward the SEI layer, contributing to good SEI stability. The smaller $R_{ct}$ of the half-cells assembled with $(PAA/ZrO_2)_3$-modified PE separator indicates faster charge transfer at electrolyte/electrode interface, which is partially attributed to the considerable $Li^+$ transference number of $(PAA/ZrO_2)_3$-modified PE separator. A large $Li^+$ transference number can effectively reduce the concentration polarization in the vicinity


DOI: 10.1021/acsami.5b05457
ACS Appl. Mater. Interfaces 2015, 7, 20678−20686

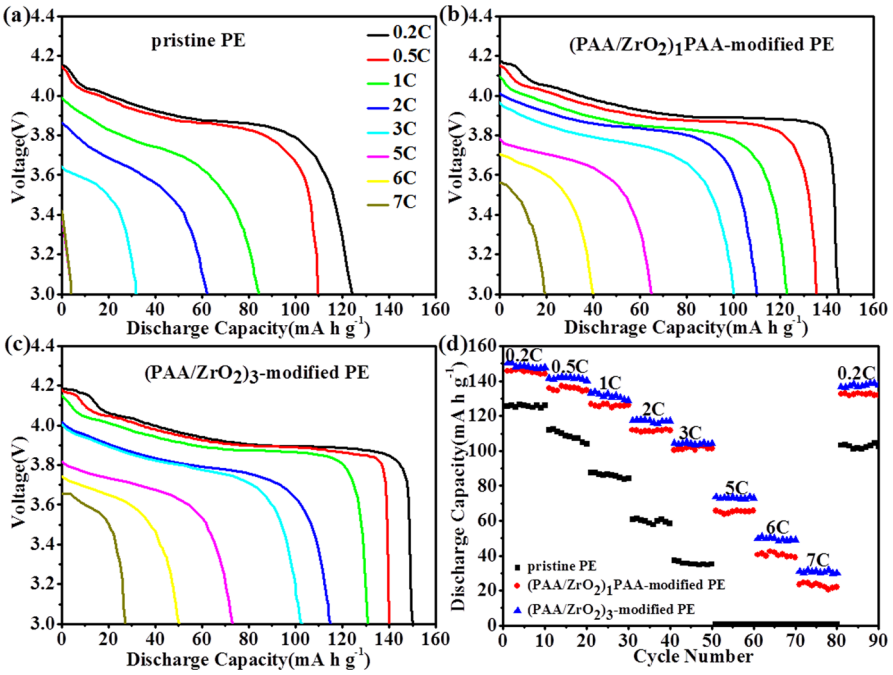


**Figure 6.** Discharge profiles of half-cells assembled with (a) pristine PE separator, (b) $(PAA/ZrO_2)_1$PAA-modified PE separator, (c) $(PAA/ZrO_2)_3$-modified PE separator, and (d) comparison of discharge capacities and C-rate capabilities, where charge/discharge current densities are varied from 0.2/0.2−7/7 C under a voltage range between 3.0 and 4.2 V.

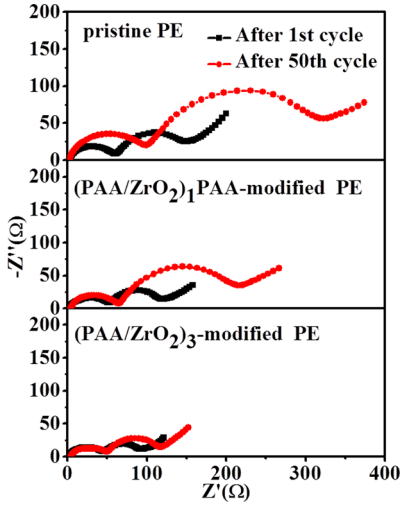


**Figure 7.** Nyquist plots of half-cells assembled with different separators after the first and 50th cycle: (a) pristine PE, (b) $(PAA/ZrO_2)_1$PAA-modified PE and (c) $(PAA/ZrO_2)_3$-modified PE.

**Table 2. Resistance Data of Half-Cells Assembled with Pristine and Modified PE Separators**

| | after 1st cycle | | | after 50th cycle | | |
|---|---|---|---|---|---|---|
| sample | $R_e$ (Ω) | $R_{SEI}$ (Ω) | $R_{ct}$ (Ω) | $R_e$ (Ω) | $R_{SEI}$ (Ω) | $R_{ct}$ (Ω) |
| pristine PE | 2.32 | 60 | 149 | 2.72 | 98 | 323 |
| $(PAA/ZrO_2)_1$PAA-modified PE | 1.81 | 52 | 120 | 2.05 | 65 | 217 |
| $(PAA/ZrO_2)_3$-modified PE | 1.69 | 47 | 92 | 1.78 | 49 | 117 |

of electrodes which is caused by the accumulation of anions to facilitate $Li^+$ ions intercalation/deintercalation, and this is particularly advantageous for lithium-ion batteries to work under high current density.[33,34] The increased $R_{SEI}$ and $R_{ct}$ values also account for the capacity decay during cycling. Therefore, it is actually the stabilized SEI layer formation and large $Li^+$ transference number that suppress the concentration polarization in the vicinity of electrodes and therefore lower the cell internal resistance, which eventually render the cell employing $(PAA/ZrO_2)_3$-modified PE separator higher capacity retention relative to $(PAA/ZrO_2)_1$PAA-modified PE separator and pristine PE separator.

## 4. CONCLUSIONS

A simple layer-by-layer (LbL) self-assembly process of poly(acrylic acid) (PAA) and $ZrO_2$ was applied to construct functional ultrathin multilayers on commercial PE separators without increasing the total thickness and sacrificing the porous structure. The LbL self-assembly method provides a unique tool for exploring the effects of top layer of modification on the separator properties and lithium-ion half-cells electrochemical performances by different deposition cycles and different top layer exposing to electrolyte. The $PAA/ZrO_2$ LbL-modified PE separators show significant improvements on a variety of crucial physical and electrochemical properties, such as the electrolyte affinity, the electrolyte uptake, the ionic conductivity, $Li^+$ transference number, the electrochemical stability and the compatibility with lithium metal electrode. The analysis results reveal that different top layers of modification (i.e., PAA or $ZrO_2$) can affect the ionization and dissociation of liquid electrolyte and the formation of solid electrolyte SEI layer. The $LiCoO_2$/Li half-cell assembled with $(PAA/ZrO_2)_3$-modified PE separator possesses the excellent capacity retention at high C-rates and the superior cycle performance due to a more stabilized SEI formation and a higher $Li^+$ transference number caused by $ZrO_2$ top layer. The simple and universal LbL self-assembly will be a promising method to solve the surface property issues on separators, and it provides the possibility for


DOI: 10.1021/acsami.5b05457
ACS Appl. Mater. Interfaces 2015, 7, 20678−20686

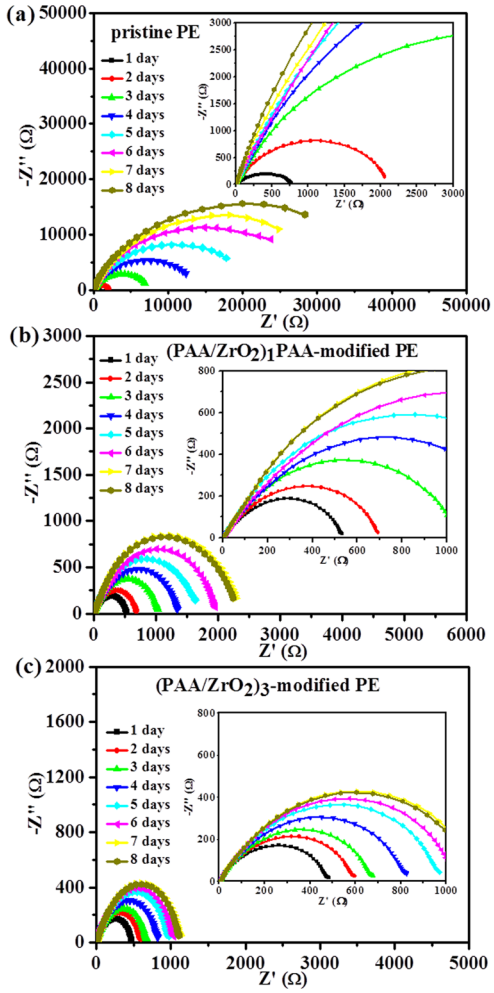


**Figure 8.** AC impedance spectra of Li/separator/Li cells based on different separators: (a) pristine PE, (b) $(PAA/ZrO_2)_1$PAA-modified PE, (c) $(PAA/ZrO_2)_3$-modified PE. (Insets) Magnified views.

the modified separator to be used in the lithium ion battery using Li metal as anode material.

## ■ ASSOCIATED CONTENT

### Supporting Information

The Supporting Information is available free of charge on the ACS Publications website at DOI: 10.1021/acsami.5b05457.

Water contact angle; liquid electrolyte wettability; thermal shrinkage for the pristine and $(PAA/ZrO_2)$ LbL-modified PE separators; linear sweep voltammetry profiles of SS/separator/Li cells for pristine PE separator and $PAA/ZrO_2$ LbL-modified PE separators; cycle performance of $LiCoO_2$/separator/Li half-cells assembled with pristine PE, $(PAA/ZrO_2)_1$PAA-modified PE or $(PAA/ZrO_2)_3$-modified PE separators; EDS elemental map of the surface of $(PAA/ZrO_2)_3$-modified PE separator disassembled from cells after 50 cycles. (PDF)

## ■ AUTHOR INFORMATION

### Corresponding Authors

*E-mail: bamboo2009@shu.edu.cn.

*E-mail: s.yuan@shu.edu.cn. Tel: +86 21 66136082.

### Notes

The authors declare no competing financial interest.

## ■ ACKNOWLEDGMENTS

The authors acknowledge Professor Kristina Edström and Torbjörn Gustafsson of Uppsala University for the helpful discussion, and National Natural Science Foundation of China (21503131), Natural Science Foundation of Shanghai (13ZR1454400), International cooperation fund of Shanghai Science and Technology Committee (14520722200), Shanghai Municipal Science and Technology Commission (13DZ2292100, 14520500200) for financial support.

## ■ REFERENCES

(1) Armand, M.; Tarascon, J. M. Building Better Batteries. *Nature* **2008**, *451*, 652−657.

(2) Thackeray, M. M.; Wolverton, C.; Isaacs, E. D. Electrical Energy Storage for Transportation Approaching the Limits of, and Going Beyond, Lithium Ion Batteries. *Energy Environ. Sci.* **2012**, *5*, 7854−7863.

(3) Liu, C.; Li, F.; Ma, L. P.; Cheng, H. M. Advanced Materials for Energy Storage. *Adv. Mater.* **2010**, *22*, E28−E62.

(4) Arora, P.; Zhang, Z. M. Battery Separators. *Chem. Rev.* **2004**, *104*, 4419−4462.

(5) Zhang, S. S. A Review on the Separators of Liquid Electrolyte Li-Ion Batteries. *J. Power Sources* **2007**, *164*, 351−364.

(6) Lee, Y.; Ryou, M. H.; Seo, M.; Choi, J. W.; Lee, Y. M. Effect of Polydopamine Surface Coating on Polyethylene Separators as a Function of Their Porosity for High-Power Li-Ion Batteries. *Electrochim. Acta* **2013**, *113*, 433−438.

(7) Ciszewski, A.; Kunicki, J.; Gancarz, I. Usefulness of Microporous Hydrophobic Polypropylene Membranes after Plasma-Induced Graft Polymerization of Acrylic Acid for High-Power Nickel-Cadmium Batteries. *Electrochim. Acta* **2007**, *52*, 5207−5212.

(8) Gwon, S. J.; Choi, J. H.; Sohn, J. Y.; Ihm, Y. E.; Nho, Y. C. Preparation of a New Micro-Porous Poly(methyl methacrylate)-Grafted Polyethylene Separator for High Performance Li Secondary Battery. *Nucl. Instrum. Methods Phys. Res., Sect. B* **2009**, *267*, 3309−3313.

(9) Kim, K. J.; Kwon, H. K.; Park, M. S.; Yim, T.; Yu, J. S.; Kim, Y. J. Ceramic Composite Separators Coated with Moisturized $ZrO_2$ Nanoparticles for Improving the Electrochemical Performance and Thermal Stability of Lithium Ion Batteries. *Phys. Chem. Chem. Phys.* **2014**, *16*, 9337−9343.

(10) Wang, S. H.; Hou, S. S.; Kuo, P. L.; Teng, H. Poly(ethylene oxide)-co-Poly(propylene oxide)-Based Gel Electrolyte with High Ionic Conductivity and Mechanical Integrity for Lithium Ion Batteries. *ACS Appl. Mater. Interfaces* **2013**, *5*, 8477−8485.

(11) Kim, K. J.; Kim, J. H.; Park, M. S.; Kwon, H. K.; Kim, H.; Kim, Y. J. Enhancement of Electrochemical and Thermal Properties of Polyethylene Separators Coated with Polyvinylidene Fluoride Hexafluoropropylene co-Polymer for Li-Ion Batteries. *J. Power Sources* **2012**, *198*, 298−302.

(12) Park, J. H.; Park, W.; Kim, J. H.; Ryoo, D.; Kim, H. S.; Jeong, Y. U.; Kim, D. W.; Lee, S. Y. Close-Packed Poly(methyl methacrylate) Nanoparticle Arrays-Coated Polyethylene Separators for High-Power Lithium Ion Polymer Batteries. *J. Power Sources* **2011**, *196*, 7035−7038.

(13) Jeong, H. S.; Hong, S. C.; Lee, S. Y. Effect of Microporous Structure on Thermal Shrinkage and Electrochemical Performance of $Al_2O_3$/Poly(vinylidene fluoride hexafluoropropylene) Composite Separators for Lithium Ion Batteries. *J. Membr. Sci.* **2010**, *364*, 177−182.

(14) Jeong, H. S.; Lee, S. Y. Closely Packed $SiO_2$ Nanoparticles/Poly(vinylidene fluoride hexafluoropropylene) Layers-Coated Polyethylene Separators for Lithium Ion Batteries. *J. Power Sources* **2011**, *196*, 6716−6722.



DOI: 10.1021/acsami.5b05457
*ACS Appl. Mater. Interfaces* 2015, 7, 20678−20686

(15) Fu, D.; Luan, B.; Argue, S.; Bureau, M. N.; Davidson, I. J. Nano $SiO_2$ Particle Formation and Deposition on Polypropylene Separators for Lithium Ion Batteries. *J. Power Sources* **2012**, *206*, 325−333.
(16) Jeong, H. S.; Kim, D. W.; Jeong, Y. U.; Lee, S. Y. Effect of Phase Inversion on Microporous Structure Development of $Al_2O_3$/Poly(vinylidene fluoride hexafluoropropylene)-Based Ceramic Composite Separators for Lithium Ion Batteries. *J. Power Sources* **2010**, *195*, 6116−6121.
(17) Jeong, Y. B.; Kim, D. W. Effect of Thickness of Coating Layer on Polymer-Coated Separator on Cycling Performance of Lithium Ion Polymer Cells. *J. Power Sources* **2004**, *128*, 256−262.
(18) Borges, J.; Mano, J. F. Molecular Interactions Driving the Layer-by-Layer Assembly of Multilayers. *Chem. Rev.* **2014**, *114*, 8883−8942.
(19) Wang, Z.; Lu, Y.; Yuan, S.; Shi, L.; Zhao, Y.; Zhang, M.; Deng, W. Hydrothermal Synthesis and Humidity Sensing Properties of Size-Controlled Zirconium Oxide ($ZrO_2$) Nanorods. *J. Colloid Interface Sci.* **2013**, *396*, 9−15.
(20) Li, Q.; Quinn, J. F.; Caruso, F. Nanoporous Polymer Thin Films via Polyelectrolyte Templating. *Adv. Mater.* **2005**, *17*, 2058−2062.
(21) Huang, C.; Lin, C. C.; Tsai, C. Y.; Juang, R. S. Tailoring Surface Properties of Polymeric Separators for Lithium Ion Batteries by Cyclonic Atmospheric-Pressure Plasma. *Plasma Processes Polym.* **2013**, *10*, 407−415.
(22) Raghavan, P.; Zhao, X. H.; Manuel, J.; Chauhan, G. S.; Ahn, J. H.; Ryu, H. S.; Ahn, H. J.; Kim, K. W.; Nah, C. Electrochemical Performance of Electrospun Poly(vinylidene fuoride-co-hexafluoropropylene)-Based Nanocomposite Polymer Electrolytes Incorporating Ceramic Fillers and Room Temperature Ionic Liquid. *Electrochim. Acta* **2010**, *55*, 1347−1354.
(23) Subramania, A.; Kalyana Sundaram, N. T.; Sathiya Priya, A. R.; Vijaya Kumar, G. Preparation of a Novel Composite Micro-Porous Polymer Electrolyte Membrane for High Performance Li-Ion Battery. *J. Membr. Sci.* **2007**, *294*, 8−15.
(24) Liu, H. Y.; Liu, L. L.; Yang, C. L.; Li, Z. H.; Xiao, Q. Z.; Lei, G. T.; Ding, Y. H. A Hard-Template Process to Prepare Three-Dimensionally Macroporous Polymer Electrolyte for Lithium Ion Batteries. *Electrochim. Acta* **2014**, *121*, 328−336.
(25) Zhang, J.; Liu, Z.; Kong, Q.; Zhang, C.; Pang, S.; Yue, L.; Wang, X.; Yao, J.; Cui, G. Renewable and Superior Thermal-Resistant Cellulose-Based Composite Nonwoven as Lithium Ion Battery Separator. *ACS Appl. Mater. Interfaces* **2013**, *5*, 128−134.
(26) Fang, T.; Duh, J. G.; Sheen, S. R. Improving the Electrochemical Performance of $LiCoO_2$ Cathode by Nanocrystalline ZnO Coating. *J. Electrochem. Soc.* **2005**, *152*, A1701−A1706.
(27) Ryou, M. H.; Lee, Y. M.; Park, J. K.; Choi, J. W. Mussel-Inspired Polydopamine-Treated Polyethylene Separators for High-Power Li-Ion Batteries. *Adv. Mater.* **2011**, *23*, 3066−3070.
(28) Zhang, Z.; Lai, Y.; Zhang, Z.; Zhang, K.; Li, J. $Al_2O_3$-Coated Porous Separator for Enhanced Electrochemical Performance of Lithium Sulfur Batteries. *Electrochim. Acta* **2014**, *129*, 55−61.
(29) Lee, J. R.; Won, J. H.; Kim, J. H.; Kim, K. J.; Lee, S. Y. Evaporation-Induced Self-Assembled Silica Colloidal Particle-Assisted Nanoporous Structural Evolution of Poly(ethylene terephthalate) Nonwoven Composite Separators for High-Safety/High-Rate Lithium Ion Batteries. *J. Power Sources* **2012**, *216*, 42−47.
(30) Wang, X.; Gong, C.; He, D.; Xue, Z.; Chen, C.; Liao, Y.; Xie, X. Gelled Microporous Polymer Electrolyte with Low Liquid Leakage for Lithium Ion Batteries. *J. Membr. Sci.* **2014**, *454*, 298−304.
(31) Liao, Y.; Sun, C.; Hu, S.; Li, W. Anti-Thermal Shrinkage Nanoparticles/Polymer and Ionic Liquid Based Gel Polymer Electrolyte for Lithium Ion Battery. *Electrochim. Acta* **2013**, *89*, 461−468.
(32) Yim, T.; Ha, H. J.; Park, M. S.; Kim, K. J.; Yu, J. S.; Kim, Y. J. A Facile Method for Construction of a Functionalized Multi-Layered Separator to Enhance Cycle Performance of Lithium Manganese Oxide. *RSC Adv.* **2013**, *3*, 25657−25661.
(33) Kuo, P. L.; Wu, C. A.; Lu, C. Y.; Tsao, C. H.; Hsu, C. H.; Hou, S. S. High Performance of Transferring Lithium Ion for Polyacrylonitrile-Interpenetrating Cross Linked Polyoxyethylene Network as Gel Polymer Electrolyte. *ACS Appl. Mater. Interfaces* **2014**, *6*, 3156−3162.
(34) Schaefer, J. L.; Yanga, D. A.; Archer, L. A. High Lithium Transference Number Electrolytes via Creation of 3-Dimensional, Charged, Nanoporous Networks from Dense Functionalized Nanoparticle Composites. *Chem. Mater.* **2013**, *25*, 834−839.


DOI: 10.1021/acsami.5b05457
*ACS Appl. Mater. Interfaces* 2015, 7, 20678−20686